Sea Surface Gravity Waves Excited by Dynamic Ground Motions from Large Regional Earthquakes

Yoshihiro Ito[*1,2], Spahr C. Webb[2], Yoshihiro Kaneko[3,4], Laura M. Wallace[3,5], and Ryota Hino[6]

Abstract

Infragravity waves on the sea surface near coastlines are occasionally excited by static displacement caused by large local earthquakes and recorded as tsunamis. However, tsunamis induced by ground motions from seismic waves are rarely observed, especially far from earthquake focal areas. We investigated seafloor pressure variations in the infragravity band at the Hikurangi subduction zone following the M 7.8 Kaikōura and M 7.1 Te Araroa earthquakes. Anomalous infragravity waves were observed at 0.2–20 mHz at sites overlying a low-velocity accretionary wedge offshore of the east coast of New Zealand's North Island accompanying the Rayleigh-wave arrivals. The maximum amplitude of these ultra-low-frequency waves was similar to the tsunami that propagated from the earthquake focal area hours later. The amplitude of the pressure signal from these waves observed offshore varied inversely with water depth, suggesting that sea surface gravity waves were excited by Rayleigh or Love waves amplified within the accretionary wedge.

Introduction

Ocean-bottom pressure recorders (OBPRs) are powerful tools for measuring ground motions over a wide spectral range, including permanent and dynamic ground motions, and also to observe tsunamis, and ocean tides and mesoscale eddies (e.g., Webb, 1998; Matsumoto *et al.*, 2018). The large dynamic range of pressure recorders ensure these signals never saturate. Signals from quasi-permanent displacements and dynamic ground motions have been observed on OBPRs at several subduction zones. Coseismic displacement exceeding 5 m was observed at one ocean-bottom pressure (OBP) gauge near the Japan trench, in response to the 2011 Tohoku–Oki earthquake (Ito *et al.*, 2011). Small displacements of several centimeters occurring over 2–4 weeks were also observed offshore northern Japan, possibly due to slow-slip events (SSEs; Ito *et al.*, 2013). Kubota *et al.* (2017) calculated centroid moment tensor inversions using dynamic pressure seismograms from the seafloor in the 5–50 -mHz band from **M** 7 class local earthquakes.

The Hikurangi margin offshore the North Island of New Zealand has been the site of rolling deployments of OBPR instruments for the last several years (Fig. 1). The Hikurangi Plateau, a Cretaceous Large Igneous Province, subducts beneath the North Island along the Hikurangi trough, east of the island. The northern Hikurangi margin is characterized by tectonic erosion and is impacted by seamounts on the subducting Pacific plate (Barnes and de Lépinay, 1997; Bell *et al.*, 2010). The highly variable seismic reflections near the

subduction interface and within the wedge are thought to be related to seamount subduction and sediment underplating (Bell *et al.*, 2010). SSEs occur proximal to the seamounts every 1–2 yr at the northern Hikurangi subduction zone, where the Hikurangi Plateau subducts westward beneath the eastern North Island along the Hikurangi trough (Wallace *et al.*, 2012, 2016). Uplift of the seafloor, on the order of 1–5 cm, was observed during a 2014 SSE with an OBPR network deployed along the northern Hikurangi margin (Wallace *et al.*, 2016; Muramoto *et al.*, 2019).

Two large earthquakes struck New Zealand in 2016; the 13 November 2016 **M** 7.8 Kaikōura earthquake and the 2 September 2016 **M** 7.1 Te Araroa earthquake (Fig. 1). Both earthquakes generated tsunami (Bai *et al.*, 2017; Kubota *et al.*, 2018). SSEs were dynamically triggered in this region following the Kaikōura earthquake (Fig. 1) (Wallace *et al.*, 2017), and an ongoing SSE was reinvigorated by the Te Araroa earthquake (Koulali *et al.*, 2017). Anomalously long durations of long-period ground motions at 10–100 mHz were observed,

1. Disaster Prevention Research Institute, Kyoto University, Uji, Kyoto, Japan; 2. Lamont–Doherty Earth Observatory, Columbia University, Palisades, New York, U.S.A.; 3. GNS Science, Avalon, Lower Hutt, New Zealand; 4. Department of Geophysics, Kyoto University, Kyoto, Japan; 5. University of Texas Institute for Geophysics, Austin, Texas, U.S.A.; 6. Graduate School of Science, Tohoku University, Sendai, Miyagi, Japan

*Corresponding author: ito.yoshihiro.4w@kyoto-u.ac.jp
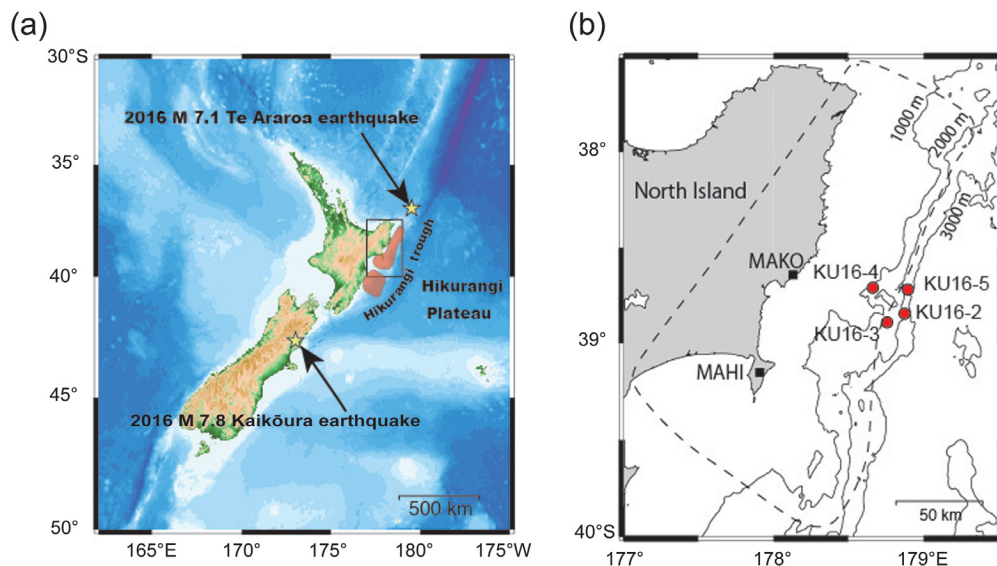
Figure 1. Map of the study region. (a) Epicenters of two large earthquakes and slow-slip events (SSEs) triggered by the 2016 **M** 7.8 Kaikōura earthquake. Yellow stars correspond to epicenters (GeoNet; see Data and Resources) and red shading indicates the areas of SSEs (Wallace *et al.*, 2017). (b) Seismic station locations. Red circles and black squares show the locations of ocean-bottom pressure recorders (OBPRs) and high-rate Global Positioning System (GPS), respectively. Solid contours show the bathymetry (General Bathymetric Chart of the Oceans [GEBCO]; see Data and Resources), and broken contours show the low-velocity accretionary wedge (Kaneko *et al.*, 2019).

especially after the Kaikōura earthquake, at seismic stations on the east coast of the North Island (Fig. 2; Kaneko *et al.*, 2019). Similar long-lasting ground motions were also observed at offshore OBPRs (Fig. 2; Kaneko *et al.*, 2019). Both Wallace *et al.* (2017) and Kaneko *et al.* (2019) concluded that the dynamic stress changes caused by the long-lasting and large-amplitude seismic waves triggered the SSEs 250–600 km away from the epicenter of the Kaikōura earthquake.

Tsunami waves usually form due to static deformation from fault ruptures, but dynamic ground deformation from the propagation of Rayleigh or Love waves, is also a potential source of sea surface gravity waves (i.e., tsunami). Ohmachi *et al.* (2001) investigated the effects of dynamic ground motions, such as Rayleigh waves, and concluded that such motions can cause sea surface gravity waves that precede the arrival time of the primary tsunami wave excited directly by static deformation in the rupture zone. Although there have been a few reports of sea surface gravity waves excited by dynamic ground motions from near-field large earthquakes, excitation of sea surface waves by earthquakes at regional distances has rarely been observed as amplitudes of Rayleigh waves decays with epicentral distance (Ohmachi *et al.*, 2001). One of the few examples of excitation at regional distances is from the large Tohoku earthquake, which excited sea surface gravity waves in the vicinity of the Dense Oceanfloor Network System for Earthquakes and Tsunamis array (Nosov *et al.*, 2015).

Sea surface gravity waves, with bottom pressure frequencies less than 30 mHz, are described as being in the infragravity wave band. The waves in the infragravity wave band are the most energetic near the shore and are usually driven by nonlinear mechanisms from short-period ocean waves near the coast (Webb *et al.*, 1991). The nonlinear interaction of different components of the infragravity wavefield can couple energy into Earth normal modes and Rayleigh waves especially near continental shelves in shallow water depths (e.g., Bertin *et al.*, 2018). Such behaviors emphasize the importance of understanding wavefields in the infragravity band observed at the seafloor. Here, we present observations in the infragravity band from OBPRs after the 2016 Kaikōura and 2016 Te Araroa earthquakes in New Zealand; our results reveal that the infragravity waves were induced by seismic waves from these large regional earthquakes.

Data and Methods
Data acquisition
Four OBPRs were deployed along the northern Hikurangi margin from June 2016 to June 2017 to investigate offshore SSEs and their relationships to earthquakes and interseismic coupling along the margin (Fig. 1). These gauges were deployed at water depths ranging from 1000 to 2500 m using the New Zealand Research Vessel (R/V) Tangaroa. An absolute pressure gauge produced by Paroscientific Inc. (United States) (Polster *et al.*, 2009) was used to record the continuous absolute pressure variations for one year, with a logging interval at either 1 or 2 s. Further descriptions of our OBPR systems are provided in detail by Hino *et al.* (2014).

Converting OBPR data to seismograms
Dynamic pressure changes caused by seismic-wave motions observed by seafloor pressure gauges can be converted to the acceleration of the ground motion assuming Rayleigh-wave propagation. The conversion is applied based on both the frequency of the ground motion and the water depth (H) of the OBP station for frequencies below the fundamental acoustic resonant frequency: $f_0 = c_0/(4H)$, in which c_0 is the velocity of marine acoustic waves (e.g., Webb, 1998; Bolshakova *et al.*, 2011;
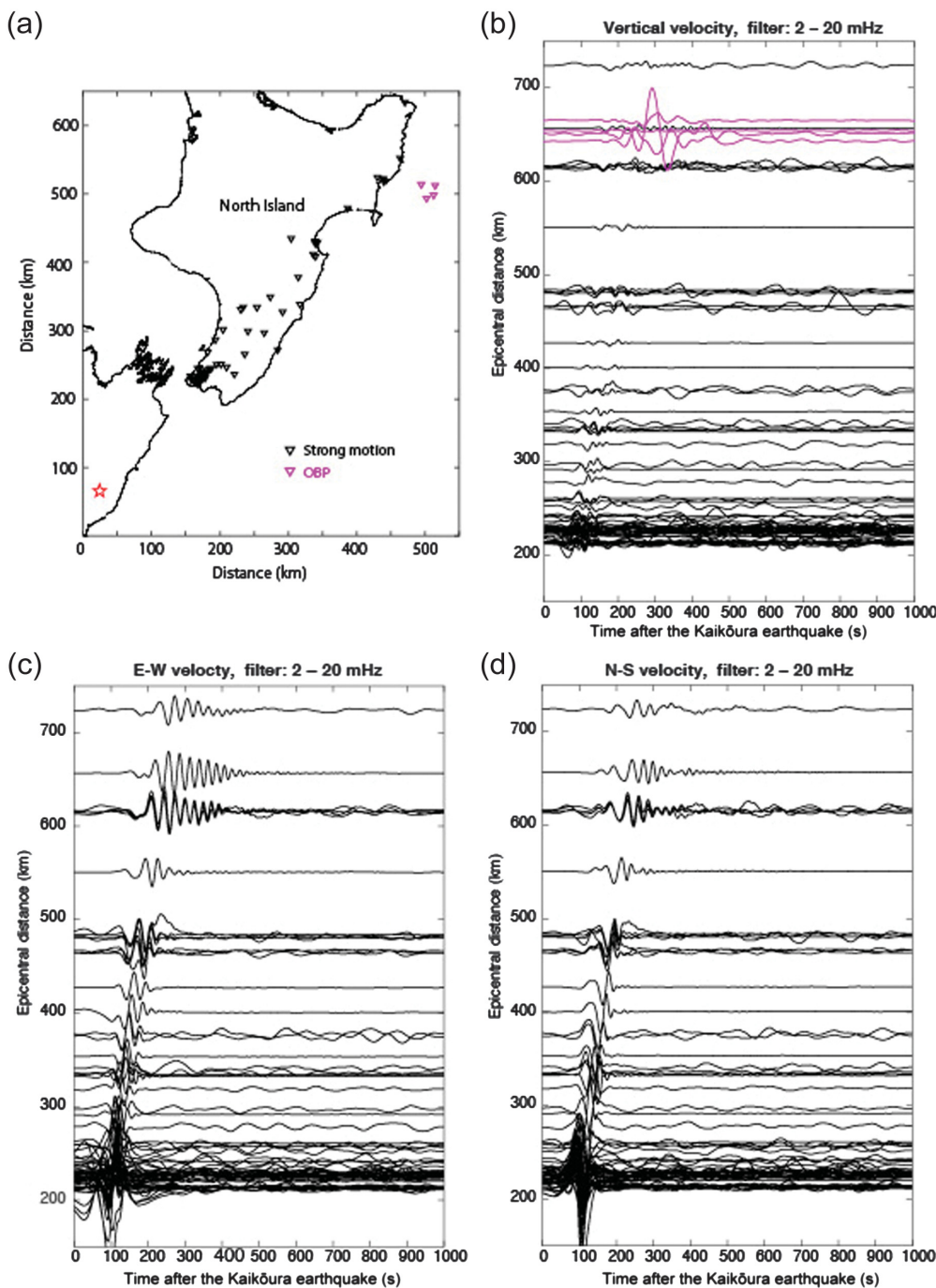
Figure 2. Long durations of long-period ground motion in the northeastern North Island of New Zealand following the **M** 7.8 Kaikōura earthquake. (a) Map of the study region. The inverted triangles show strong motion (black), and ocean-bottom pressure (OBP) gauge sites (pink). The star corresponds to the epicenter of the Kaikōura earthquake. Seismic record sections showing (b) vertical, (c) east–west, and (d) north–south components of particle velocities filtered between 2 and 50 mHz. Strong motion (black) and OBP gauges (pink) waveforms are shown. All the traces are scaled by a constant value and hence are on the same amplitude scale.

ground motion a at the sea-floor can be approximated from the dynamic pressure change p as follows:

$$a(f) \simeq p(f)/\rho H(f < f_0), \quad (1)$$

in which ρ is the density of seawater. We assumed a seawater density $\rho = 1026\,\text{kg/m}^3$. The fundamental acoustic resonant frequencies f_0 at the shallowest and deepest stations were ~0.4 and ~0.1 Hz, respectively, for an acoustic velocity $c_0 = 1.5$ km/s.
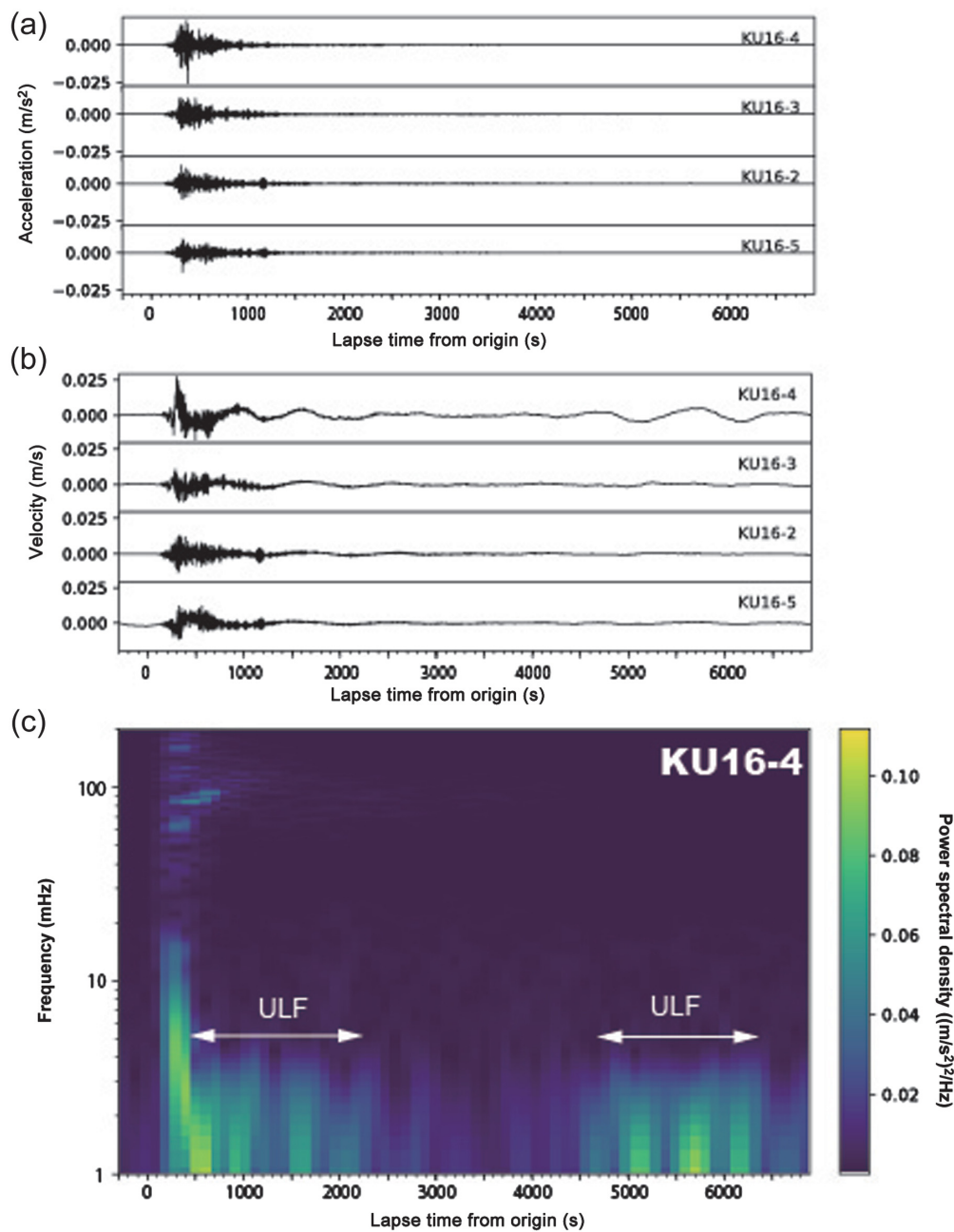
Spectral analysis

Power spectra and spectrograms were generated from the seismograms calculated on the OBPR data. To calculate robust spectra for seismogram data, we applied a multi-window spectral method (Imanishi and Ellsworth, 2006). For each OBPR time record, we first calculated the Fourier spectral amplitudes in a tapered 2000 s time window. This calculation was then repeated along the OBPR time series in every 10 s step of the moving the time window. The total number of moving time windows was 50, with a total length of 2500 s. Finally, all the spectra for the same event or noise pair were stacked. To generate spectrograms, we used a tapered, 512 s time window in which the time window was moved in 410 s steps.

Results and Discussion
Analysis of OBPR data

Large ground motions lasting more than 500 s were observed at all the OBPRs as the 2016 Kaikōura earthquake wave train passed through the region (e.g., Kaneko *et al.*, 2019). In addition, there were two ultra-low-frequency (ULF) waves (<10 mHz) in the velocity

Matsumoto *et al.*, 2012; Kubota *et al.*, 2017; Saito, 2017). When the frequency of ground motion, or the acoustic frequency, f is sufficiently low compared to f_0, the vertical acceleration of the

Figure 3. Seismic records and spectrogram observed after the 2016 Kaikōura earthquake. (a) Accelerogram converted from seafloor pressure records at 1–200 mHz. (b) Velocity seismograms inferred from pressure records at 1–200 mHz. (c) Spectrogram in velocity at site KU16-4. White double arrows indicate two ultra-low-frequency (ULF) waves lasting from 500 to 2500 s and 4500 to 6500 s after the origin time.
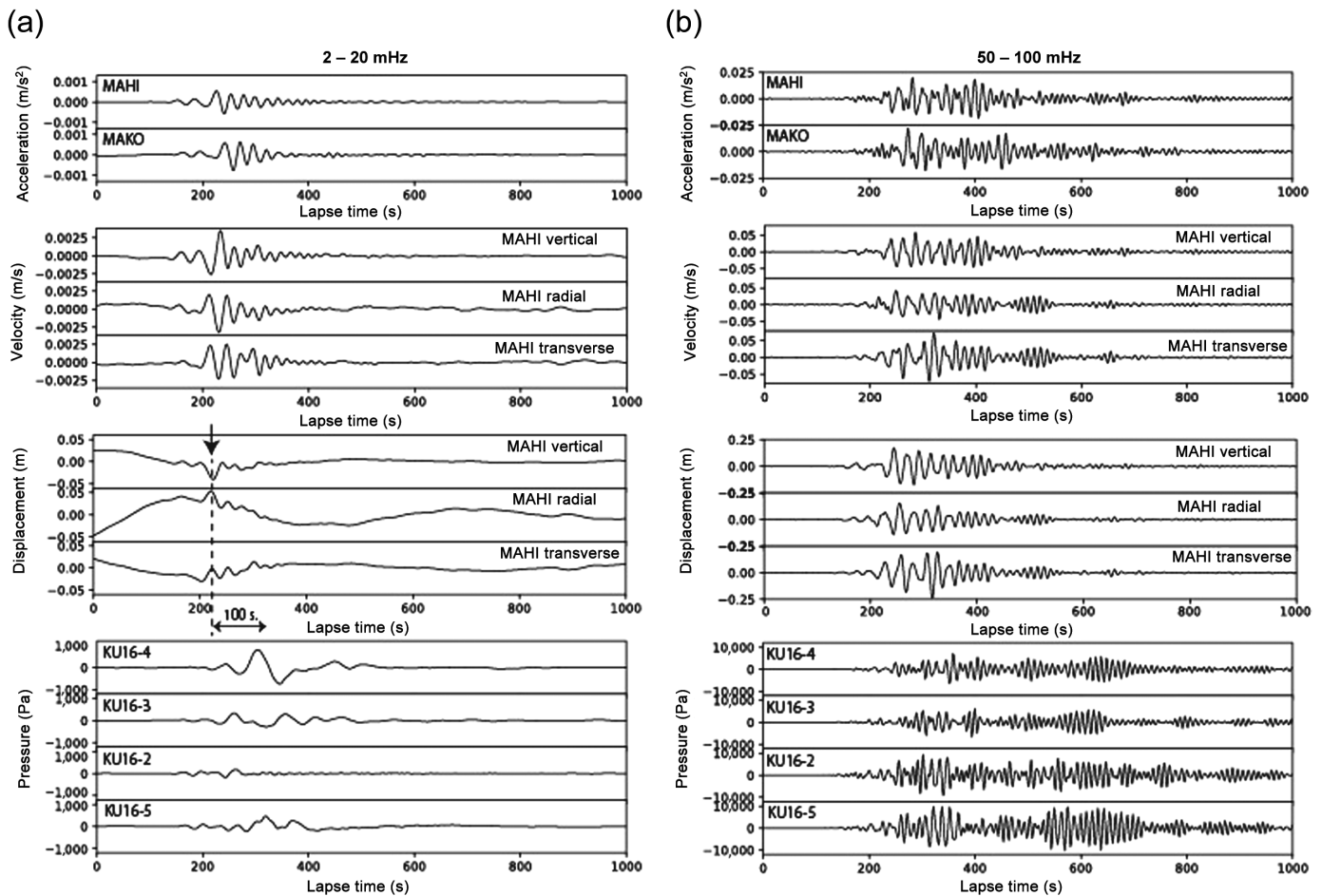
variations from the tsunami with a velocity of ~0.1 km/s, radiating from the source area of the mainshock 500 km away from the OBPR network. The first ULF wave is too early to be a tsunami from the static crustal displacement from the mainshock. This implies that the origin of its excitation is likely in the area of the OBPR sites.

The first ULF wave accompanies the arrival of the surface waves that have a dominant frequency of 2–20 mHz (Fig. 3). The largest amplitude of the ULF waves at the OBPRs occurs shortly after the arrival of surface waves (Figs. 2 and 4). The waveform of the ULF waves on KU16-4, which is closest to the coastline, is similar to Rayleigh waves observed as the vertical and radial displacements observed at MAHI (Fig. 4), but with an inverted polarity and longer period, because increasing pressure indicates downward motion at a site. The vertical displacement at MAHI shows a time advance of ~100 s relative to the waveform at KU16-4, which is not consistent with seismic surface-wave propagation, given the ~70–80 km difference in the epicentral distances. Clear surface waves were observed at both onshore and offshore seismometer sites in the 50–100 mHz band, producing long-duration and high-amplitude ground motions lasting for 200–400 s (Kaneko *et al.*, 2019). These observations suggest that the first ULF waves observed on the OBPRs at 2–20 mHz are associated with the oceanic water layer above the OBPRs, as no ULF waves are observed at onshore sites.

After the 2016 **M** 7.1 Te Araroa earthquake, similar ULF waves to those from the Kaikōura earthquake were observed on the same OBPR network (Figs. 5 and 6). Three ULF waves

seismograms (derived from the pressure records), especially at site KU16-4, at 300–2500 and 4500–6500 s from the origin (Fig. 3). The first UFL wave in the infragravity wave band is identified immediately after the arrival of the surface wave from the mainshock and continues to at least 2500 s from the origin in the spectrogram (Fig. 3c). The second ULF wave arrives 4500 s after the mainshock, and is due to the pressure

(a)

(b)

were observed, the first of which was recorded near the lapse time of ∼150 s; it had the same spectral structure as that observed after the Kaikōura earthquake. The second and the third waves were observed at ∼1800 and ∼5500 s, respectively. The latter two waves correspond to the phase arrivals of direct tsunami from the source area of the mainshock and a reflected tsunami wave from the east coast of the North Island (Kubota *et al.*, 2018). The first set of ULF waves was observed immediately after the arrival of body or early surface waves, and before the arrival of the two tsunami phases radiated from the source region.

The ULF waves following the 2016 Kaikōura earthquake, and the 2016 Te Araroa earthquake exhibited a water depth dependence in amplitude (Fig. 7). The largest amplitude in pressure was observed at the shallowest site, with a water depth of 1049 m. The amplitude in the 2.5–5, 5–10, 10–20 mHz bands from the earthquakes decreased with the increasing water depth of the OBPR site. In contrast, the amplitudes of 20–40 and 20–40 mHz observations following the Kaikōura earthquake and 40–80 mHz observations following the Te Araroa earthquake also varied with water depth, but with the largest amplitude observed at the deepest site, KU16-5 (at 2468 m). The amplitude of the ULF (infragravity wave band) waves offshore was observed to be roughly inversely

Figure 4. ULF (infragravity) waves following the **M** 7.8 Kaikōura earthquake on onshore and offshore sites. (a) Top: Onshore accelerograms from high-rate displacement time series at two GPS sites, MAHI, and MAKO (location shown on Fig. 1); middle: velocity seismograms at MAHI; and lower: offshore pressure records at 2–20 mHz in the infragravity band. A downward arrow and dashed line indicate Rayleigh wave. A left–right arrow indicates a time difference of 100 s. (b) Same as (a) but in the 50–100 mHz band (above the infragravity band).

proportional to the water depth at each OBPR site, and approximately proportional to the water depth in the higher frequency bands (Fig. 7). The spectral amplitude increases with depth for higher frequencies may be explained with equation (1), assuming that the ground accelerations across the OBPR network were similar (i.e., nearly constant). This suggests that the pressure observations at high frequencies (> ∼ 0.1 Hz) were dominated by an elastically induced (seismic) motion of the seafloor.

Amplitudes in the infragravity wave band on power spectral densities between 2 and 20–40 mHz showed no obvious frequency dependence, whereas amplitude increased as a function of frequency at the higher frequencies of 20 and 40 mHz in the Kaikōura and Te Araroa earthquakes (Fig. 8). The Fourier
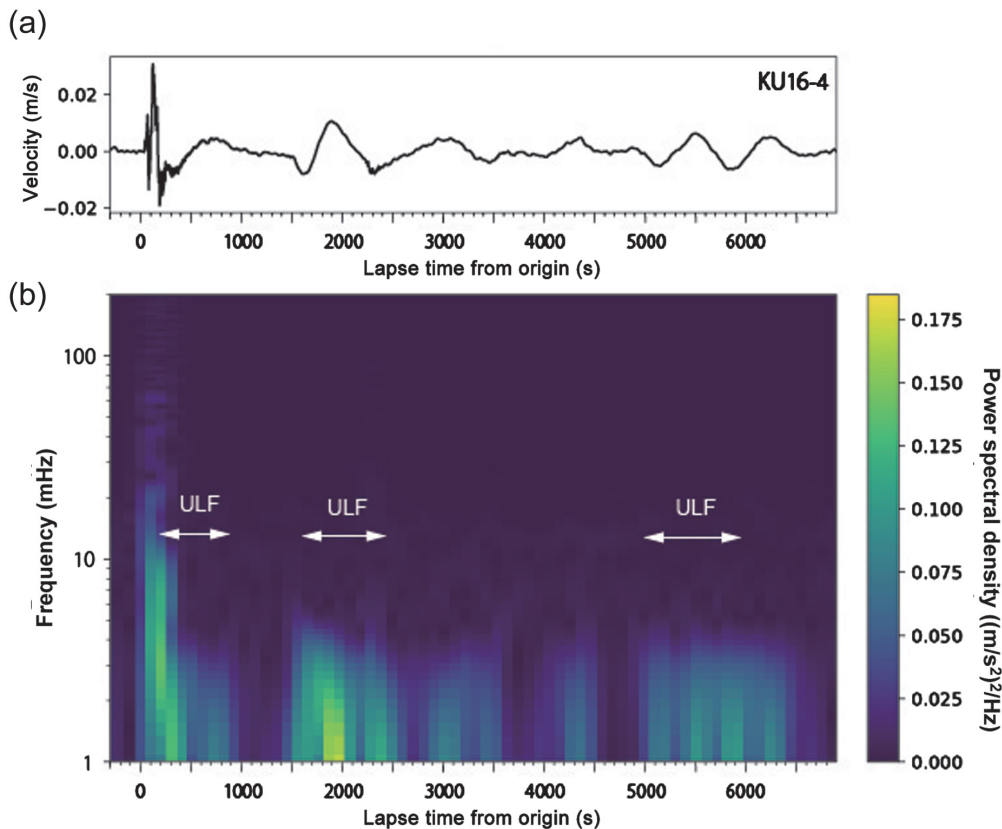
Figure 5. (a) Seismogram and (b) spectrogram observed after the 2016 M 7.1 Te Araroa earthquake at site KU16-4 (OBPR). White double arrows indicate three ULF waves lasting from 150–900 s, 1500–1900 s, and 5500–6400 s after the origin time.

spectral amplitude for long-period Rayleigh waves from an earthquake source generally increases as frequency to the fourth power (in acceleration), which is consistent with the observed spectra in a frequency range of $20 \sim 40$–100 mHz. This further supports the idea that pressure records in this bandwidth were dominated by the solid earth surface-wave ground motion. The lower frequency waves (>20–40 mHz) observed after the Kaikōura and Te Araroa earthquakes, however, show no easily interpretable frequency dependence, although the spectra from KU16-2 near the trench show some slight frequency dependence.

Infragravity wave coupling

The inverse proportionality of ULF wave amplitudes with water depth (i.e., depth dependency) observed in this study may be explained by coupling between Rayleigh or Love waves and infragravity surface waves through interaction with seafloor bathymetry similar to the mechanism believed to excite single frequency (or primary) microseisms (Hasselmann, 1963; Ardhuin, 2018). We can only observe the Rayleigh waves in the seafloor pressure data, but Rayleigh and Love waves will arrive at very similar times, so coupling between Love waves and sea

surface waves may also contribute to the signals we detect. In this mechanism, infragravity waves interact with a component of the seafloor bathymetry with similar wavenumbers to couple energy into seismic waves of the same frequency, but much higher phase velocity. The coupling should be bidirectional so that highly energetic Rayleigh or Love waves interacting with bathymetry may also couple energy into infragravity waves. Ardhuin et al. (2015) suggests a roughly inverse depth dependence for the horizontal point-force component of this single frequency microseism mechanism for frequencies for which sea surface-wave wavelengths are large compared to the water depth.

Infragravity waves with frequencies of 2–20 mHz have wavelengths of $\sim$5–90 km in water depths of 1–3 km (as relevant to the study area). The wavelengths of the sea surface waves are roughly consistent with a 100–500 km width of the region with the low-velocity sediment layer exciting long-duration motions at 10–100 mHz (Kaneko et al., 2019), as well as to the area of slow slip triggered by the Kaikōura earthquake (Fig. 1) (Wallace et al., 2017). The long-duration motions observed onshore and offshore were distributed within epicentral distances between 580 and 730 km along the east coast of the North Island, where an extremely low-velocity accretionary wedge above the plate interface is required to produce the observed long-period ground motions, and this contributed to the triggering of the SSEs (Kaneko et al., 2019). The sea surface waves observed after the two regional earthquakes were excited just above this wedge, and these excited sea surface gravity waves caused pressure variations at the seafloor, which were observed in the infragravity band at less than 20–40 mHz.

The amplifying effects of sedimentary basins on strong ground motions have been recognized in other subduction zones. Similar effects to those reported here have been shown within sedimentary basins as resonance periods of 7–12 s in Kanto, Japan (Furumura and Hayakawa, 2007), and 2–3 s in the basin of Mexico City using seismograms (Cruz-Atienza et al., 2016). Nakamura et al. (2015) also demonstrated amplified
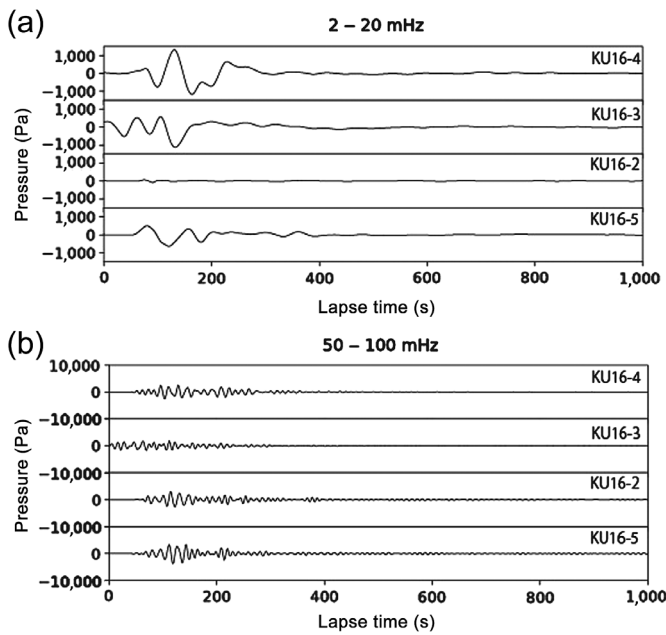
Figure 6. Offshore pressure records at (a) 2–20 mHz of the infragravity band and (b) at 50–100 mHz higher than the infragravity band after the 2016 **M** 7.1 Te Araroa earthquake.

offshore seismograms in a low-velocity accretionary wedge along the Nankai trough, Japan. These observations suggest surface waves amplified within a low-velocity accretionary wedge or a basin filled with low-velocity sediments under a water layer.

The infragravity waves observed from seafloor pressures at shallow water depth (<1000 m depth) may induce errors into the estimates derived from source models of tsunamis. The observed amplitudes of the sea surface gravity waves were 1000 Pa (equivalent to ~10 cm water height) in the cases of both the Kaikōura and Te Araroa earthquakes. This amplitude is large enough that its effect should be considered in tsunami modeling, especially for the early portion of tsunami waveforms at sites with shallow water depths. Indeed, the observed amplitudes of induced infragravity waves at site KU16-4 in the Kaikōura and Te Araroa earthquakes were nearly identical to those of the tsunami due to static deformation from the fault rupture (Figs. 3 and 5). Some discrepancies in tsunami models have been reported in comparisons of models with seismic and tsunami data (e.g., Shuto, 1991; Ohmachi *et al.*, 2001), which could stem from infragravity waves such as those we describe here. This suggests that careful attention must be paid to the contributions of infragravity waves in tsunami models when using regional bottom pressure data (<800 km from the source areas of large earthquakes), as well as for near-field bottom pressure data.
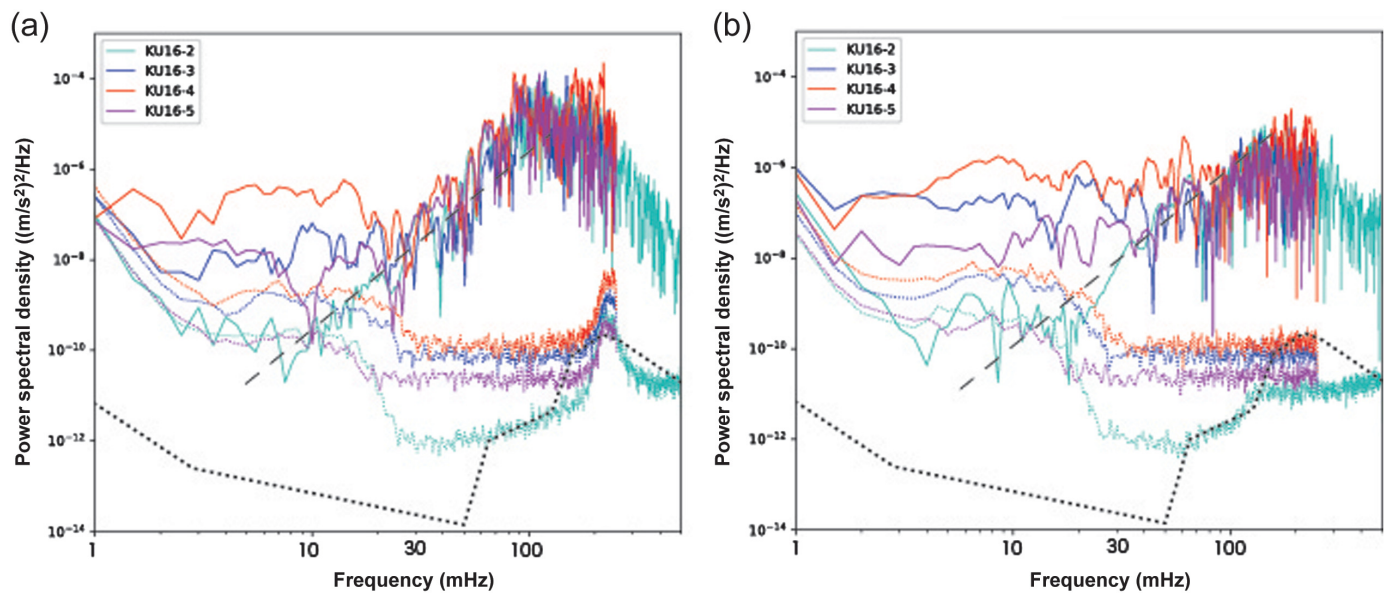
Conclusions

OBP fluctuations in the infragravity band were observed following both the 2016 **M** 7.8 Kaikōura and **M** 7.1 Te Araroa earthquakes. ULF ocean waves were observed following the arrival of Rayleigh or Love waves excited by the mainshocks. The pressure amplitude at a shallow water depth site was almost the same as that of the tsunami directly radiated from the source region and observed at the OBPR sites later. The observed pressure amplitude varied approximately inversely with depth. The observed signals were interpreted as infragravity waves (i.e., sea surface gravity waves or sea surface wave)
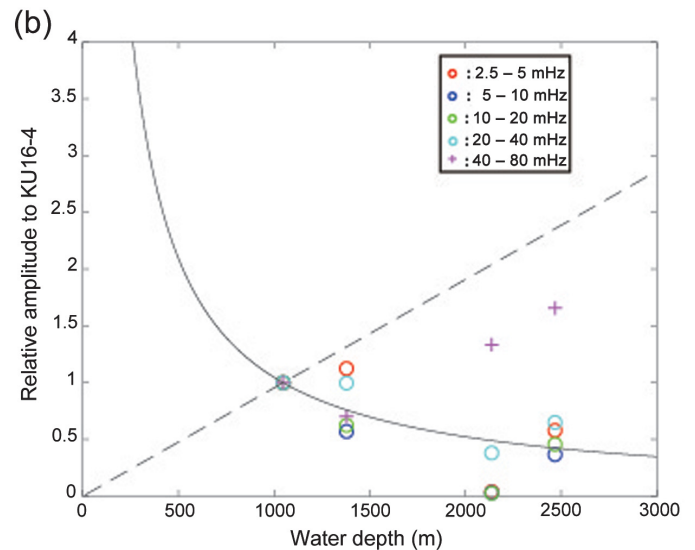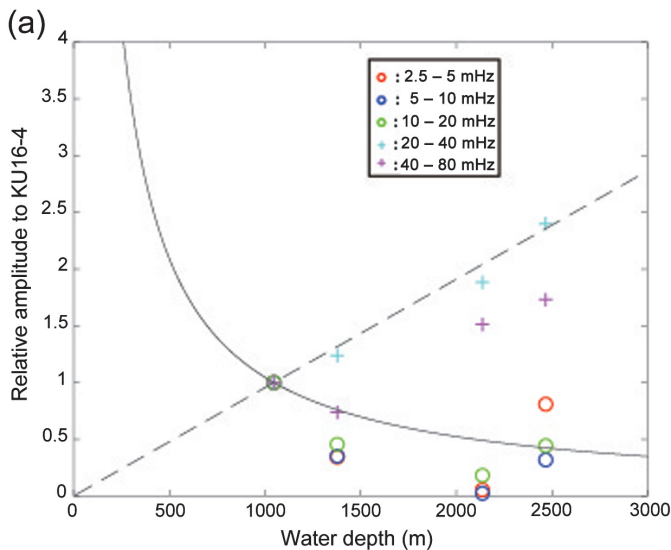
Figure 7. Depth dependence of observed pressure fluctuations for the (a) Kaikōura earthquake and (b) Te Araroa earthquake. Solid

and dashed lines indicate inverse proportionality and direct proportionality to water depth, respectively.

(a) (b)

Figure 8. Power spectral densities in acceleration observed on OBPRs for the (a) Kaikōura earthquake and (b) Te Araroa earthquake. Colored solid lines correspond to calculated power spectral densities with a time window of 1000 s, including the direct body and surface waves from the two large earthquakes. Colored stippled lines show power spectral densities calculated from noise without any seismic signal before the occurrence of the mainshock. Black stippled lines show the new high-noise model (Peterson, 1993). The typical flat spectrum at long period in displacement (e.g., Brune, 1970; Boatwright, 1978) produces a frequency to the fourth dependence for long-period earthquake spectra in acceleration (dashed line).

caused by the dynamic ground motions of Rayleigh or Love waves.

Data and Resources

The data reported in this study were recorded in our ocean-bottom pressure (OBP) gauges network, except for the high-rate Global Positioning System (GPS) and strong-motion records, which belong to New Zealand's GeoNet website (https://www.geonet.org.nz). Some plots were made using the Generic Mapping Tools version 5.3.1 (v.5.3.1; www.soest.hawaii.edu/gmt; Wessel *et al.*, 2013) and the MATLAB software v.R2018b (www.mathworks.com). GeoNet earthquake details are available at https://www.geonet.org.nz/earthquake/story. General bathymetric chart of the oceans (GEBCO) is available at https://www.gebco.net/data_and_products/gridded_bathymetry_data/. All websites were last accessed in July 2019.

References

Ardhuin, F. (2018). Large-scale forces under surface gravity waves at a wavy bottom: A mechanism for the generation of primary microseisms, *Geophys. Res. Lett.* **45,** no. 16, 8173–8181, doi: 10.1029/2018GL078855.

Ardhuin, F., L. Gualtieri, and E. Stutzmann (2015). How ocean waves rock the Earth: Two mechanisms explain microseisms with periods 3 to 300 s, *Geophys. Res. Lett.* **42,** no. 3, 765–772, doi: 10.1002/2014gl062782.

Bai, Y., T. Lay, K. F. Cheung, and L. Ye (2017). Two regions of seafloor deformation generated the tsunami for the 13 November 2016, Kaikoura, New Zealand earthquake, *Geophys. Res. Lett.* **44,** no. 13, 6597–6606, doi: 10.1002/2017GL073717.

Barnes, P. M., and B. M. de Lépinay (1997). Rates and mechanics of rapid frontal accretion along the very obliquely convergent southern Hikurangi margin, New Zealand, *J. Geophys. Res.* **102,** no. B11, 24,931–24,952, doi: 10.1029/97JB01384.

Bell, R., R. Sutherland, D. H. N. Barker, S. Henrys, S. Bannister, L. Wallace, and J. Beavan (2010). Seismic reflection character of the Hikurangi subduction interface, New Zealand, in the region of repeated Gisborne slow slip events, *Geophys. J. Int.* **180,** no. 1, 34–48, doi: 10.1111/j.1365-246X.2009.04401.x.

Bertin, X., A. de Bakker, A. van Dongeren, G. Coco, G. André, F. Ardhuin, P. bonneton, F. Bouchette, B. Castelle, W. C. Crawford, *et al.* (2018). Infragravity waves: From driving

mechanisms to impacts, *Earth Sci. Rev.* **177,** 774–799, doi: 10.1016/j.earscirev.2018.01.002.

Boatwright, J. (1978) Detailed spectral analysis of two small New York state earthquakes, *Bull. Seismol. Soc. Am.* **68,** no. 4, 1117–1131.

Bolshakova, A., S. Inoue, S. Kolesov, H. Matsumoto, M. Nosov, and T. Ohmachi (2011). Hydroacoustic effects in the 2003 Tokachi-Oki tsunami source, *Russian J. Earth Sci.* **12,** no. 2, ES2005, doi: 10.2205/2011ES000509.

Brune, J. N. (1970). Tectonic stress and the spectra of seismic shear wave from earthquakes, *J. Geophys. Res.* **75,** 4997–5009, doi: 10.1029/JB075i026p04997.

Cruz-Atienza, V. M., J. Tago, J. D. Sanabria-Gomez, E. Chaljub, V. Etienne, J. Virieux, and L. Quintanar (2016). Long duration of ground motion in the paradigmatic valley of Mexico, *Sci. Rep.* **6,** no. 1, 38807, doi: 10.1038/srep38807.

Furumura, T., and T. Hayakawa (2007). Anomalous propagation of long-period ground motions recorded in Tokyo during the 23 October 2004 Mw 6.6 Niigata-ken Chuetsu, Japan, earthquake, *Bull. Seismol. Soc. Am.* **97,** no. 3, 863–880, doi: 10.1785/0120060166.

Hasselmann, K. (1963). A statistical analysis of the generation of microseisms, *Rev. Geophys.* **1,** no. 2, 117–210, doi: 10.1029/RG001i002p00177.

Hino, R., D. Inazu, Y. Ohta, Y. Ito, S. Suzuki, T. Iinuma, Y. Osada, M. Kido, H. Fujimoto, and Y. Kaneda (2014). Was the 2011 Tohoku-Oki earthquake preceded by aseismic preslip? Examination of seafloor vertical deformation data near the epicenter, *Mar. Geophys. Res.* **35,** no. 3, 181–190, doi: 10.1007/s11001-013-9208-2.

Imanishi, K., and W. L. Ellsworth (2006). Source scaling relationships of microearthquakes at Parkfield, CA, determined using the SAFOD Pilot Hole Seismic Array, in *Earthquakes: Radiated Energy and the Physics of Earthquake Faulting, Geophysical Monograph Series*, R. Abercrombie, A. McGarr, G. Di Toro, and H. Kanamori (Editors), Vol. 170, 81–90, American Geophysical Union, Washington, D.C., doi: 10.1029/170GM10.

Ito, Y., R. Hino, M. Kido, H. Fujimoto, Y. Osada, D. Inazu, Y. Ohta, T. Iinuma, M. Ohzono, S. Miura, *et al.* (2013). Episodic slow slip events in the Japan subduction zone before the 2011 Tohoku-Oki earthquake, *Tectonophysics* **600,** 14–26, doi: 10.1016/j.tecto.2012.08.022.

Ito, Y., T. Tsuji, Y. Osada, M. Kido, D. Inazu, Y. Hayashi, H. Tsushima, R. Hino, and H. Fujimoto (2011). Frontal wedge deformation near the source region of the 2011 Tohoku-Oki earthquake, *Geophys. Res. Lett.* **38,** no. 7, L00G05, doi: 10.1029/2011GL048355.

Kaneko, Y., Y. Ito, B. Chow, L. M. Wallace, C. Tape, R. Grapenthin, E. D'Anastasio, S. Henrys, and R. Hino (2019). Ultra-long duration of seismic ground motion arising from a thick, low velocity sedimentary wedge, *J. Geophys. Res.* **124,** no. 10, 10,347–10,359, doi: 10.1029/2019JB017795.

Koulali, A., S. McClusky, L. Wallace, S. Allgeyer, P. Tregoning, E. D'Anastasio, and R. Benavente (2017). Slow slip events and the 2016 Te Araroa Mw 7.1 earthquake interaction: Northern Hikurangi subduction, New Zealand, *Geophys. Res. Lett.* **44,** 8336–8344, doi: 10.1002/2017GL074776.

Kubota, T., T. Saito, Y. Ito, Y. Kaneko, L. M. Wallace, S. Suzuki, R. Hino, and S. Henrys (2018). Using tsunami waves reflected at the coast to improve offshore earthquake source parameters: Application to the 2016 Mw 7.1 Te Araroa earthquake, New Zealand, *J. Geophys. Res.* **123,** no. 10, 8767–8779, doi: 10.1029/2018JB015832.

Kubota, T., T. Saito, W. Suzuki, and R. Hino (2017). Estimation of seismic centroid moment tensor using ocean bottom pressure gauges as seismometers, *Geophys. Res. Lett.* **44,** no. 21, 10,907–10,915, doi: 10.1002/2017GL075386.

Matsumoto, H., S. Inoue, and T. Ohmachi (2012). Dynamic response of bottom water pressure due to the 2011 Tohoku earthquake, *J. Disast. Res.* **7,** no. 7, 468–475, doi: 10.20965/jdr.2012.p0468.

Matsumoto, H., T. Kimura, S. Nishida, Y. Machida, and E. Araki (2018). Experimental evidence characterizing pressure fluctuations at the seafloor-water interface induced by an earthquake, *Sci. Rep.* **8,** no. 16406, doi: 10.1038/s41598-018-34578-2.

Muramoto, T., Y. Ito, D. Inazu, L. M. Wallace, R. Hino, S. Suzuki, S.C. Webb, and S. Henrys (2019). Seafloor crustal deformation on ocean bottom pressure records with nontidal variability corrections: Application to Hikurangi margin, New Zealand, *Geophys. Res. Lett.* **46,** 303–310, doi: 10.1029/2018GL080830.

Nakamura, T., H. Takenaka, T. Okamoto, M. Ohori, and S. Tsuboi (2015). Long-period ocean-bottom motions in the source areas of large subduction earthquakes, *Sci. Rep.* **5,** no. 1, 16648, doi: 10.1038/srep16648.

Nosov, M. A., K. A. Sementsov, S. V. Kolesov, H. Matsumoto, and B. W. Levin (2015). Recording of gravity waves formed in the ocean by surface seismic waves during the earthquake of March 11, 2011, off the coast of Japan, *Dokl. Earth Sci.* **461,**, 408–413.

Ohmachi, T., H. Tsukiyama, and H. Matsumoto (2001). Simulation of tsunami induced by dynamic displacement of seabed due to seismic faulting, *Bull. Seismol. Soc. Am.* **91,** no. 6, 1898–1909, doi: 10.1785/0120000074.

Peterson, J. (1993). *Observations and Modeling of Seismic Background Noise (Rep. 93-322)*, United States Geological Survey, Albuquerque, New Mexico, doi: 10.3133/ofr93322.

Polster, A., M. Fabian, and H. Villinger (2009). Effective resolution and drift of Paroscientific pressure sensors derived from long-term seafloor measurements, *Geochem. Geophys. Geosys.* **10,** no. 8, Q08008, doi: 10.1029/2009GC002532.

Saito, T. (2017). Tsunami generation: Validity and limitations of conventional theories, *Geophys. J. Int.* **210,** no. 3, 1888–1900, doi: 10.1093/gji/ggx275.

Shuto, N. (1991). Numerical simulation of tsunami—Its present and near future, *Nat. Hazards* **4,** nos. 2/3, 171–191, doi: 10.1007/BF00162786.

Wallace, L. M., Å. Fagereng, and S. Ellis (2012). Upper plate tectonic stress state may influence interseismic coupling on subduction megathrusts, *Geology* **40,** no. 10, 895–898, doi: 10.1130/g33373.1.

Wallace, L. M., Y. Kaneko, S. Hreinsdótti, I. Hamling, Z. Peng, N. Bartlow, E. D'Anastasio, and B. Fry (2017). Large-scale dynamic triggering of shallow slow slip enhanced by overlying sedimentary wedge, *Nat. Geosci.* **10,** no. 10, 765–770, doi: 10.1038/ngeo3021.

Wallace, L. M., S. C. Webb, Y. Ito, K. Mochizuki, R. Hino, S. Henrys, S. Y. Schwartz, and A. F. Sheehan (2016). Slow slip near the trench at the Hikurangi subduction zone, New Zealand, *Science* **352,** no. 6286, 701–704, doi: 10.1126/science.aaf2349.

Webb, S. C. (1998). Broadband seismology and noise under the ocean, *Rev. Geophys.* **36,** no. 1, 105–142, doi: 10.1029/97RG02287.

Webb, S. C., X. Zhang, and W. C. Crawford (1991). Infragravity waves in the deep ocean, *J. Geophys. Res.* **96,** 2723–2736.

Wessel, P., W. H. F. Smith, R. Scharroo, J. Luis, and F. Wobbe (2013). Generic mapping tools: Improved version released, *Eos Trans. AGU* **94,** no. 45, 409–410, doi: 10.1002/2013EO450001.